Structure and fragility in a macroscopic model of a glass-forming liquid based on a nonvibrating granular system

C. Tapia-Ignacio,[1] R. E. Moctezuma,[2] and F. Donado[1]

[1]*Instituto de Ciencias Básicas e Ingeniería, Universidad Autónoma del Estado de Hidalgo, Mineral de la Reforma 42184, Hidalgo, México*

[2]*CONACYT-Instituto de Física "Manuel Sandoval Vallarta", Universidad Autónoma de San Luis Potosí, Alvaro Obregón 64, 78000 San Luis Potosí, S.L.P., México*

(Received 9 April 2018; revised manuscript received 18 July 2018; published 11 September 2018)

We studied glass transition in a nonvibrating granular system composed of magnetic steel beads under an unsteady magnetic field. In this model system, particle concentration and effective temperature can be changed independently. We analyzed several particle concentration cases. As concentration increases, the system goes from a fragile to a strong glass-forming liquid behavior and the regularity factor increases showing that the system becomes more regular. As the effective potential shows deeper wells, the fragility index decreases, and the regularity factor increases.

DOI: 10.1103/PhysRevE.98.032901

I. INTRODUCTION

When a glass-forming liquid is quickly cooled, it undergoes a glass transition. In the glassy state, the system is out of thermodynamic equilibrium and particles exhibit a slowed-down dynamic. Thus far, a direct study of the dynamics and structural characteristics of this transition has not been possible since we cannot currently track molecular particles. Consequently, macroscopic models such as colloidal and granular systems are being used to obtain information about the detailed particle behavior occurring inside the glass-forming liquid as it approaches the glassy state [1–9]. In these systems, the inverse of the particle concentration plays the role of the effective temperature. The interactions between particles are mainly due to hard sphere interactions and the structural configurations change resulting from various particle concentration. In these systems, the particles only interact when they are close enough to collide, reaching states near jamming [5,6].

In some experiments, using vibrating granular systems to model glass transition, a fragile glass-forming liquid behavior has been found [7,8]. Additionally, in Ref. [10] we have found that a nonvibrating granular system could behave as a strong glass-forming liquid. In this model system, the inter-particle interactions can be modulated by an active control, thus the interparticle interactions are strong enough to interact at long distances. From these previous findings, we infer that the length and strength of the particle interaction in granular models for a glass-forming liquid, determine its fragility. Therefore, changing particle concentration or interparticle interactions it could be possible to modify fragility in these model systems.

In this work, we studied the dynamical and structural properties of a nonvibrating granular system in series of experiments where it is suddenly quenched; it goes from a gaslike state to a lower temperature state that could be a fluid state or a solid state. We determined the glass transition temperature and studied the behavior of the effective viscosity near glass transition. We determined the fragility of the system for each one of several different particle concentration cases. Furthermore, we studied the structural properties of the system by means of the regularity factor obtained from Voronoi polygon area distributions. The regularity factor, which is a parameter in a two-parameter γ distribution, shows differences in structures belonging to a gas, liquid, glass, crystal, or gel such as those that have been shown in Refs. [11–17].

II. EXPERIMENTAL SETUP

The system is composed of stainless steel particles confined within a circular plate measuring 72 mm in diameter. The particle concentration is given by the surface fraction occupied by the particles, $\phi_s = \frac{\pi N \sigma^2}{4A}$, where N is the average number of particles within the field of view of area A, and σ is the particle diameter. The system is located horizontally in the middle of a pair of Helmholtz coils of 150 mm in diameter, which produce a homogeneous magnetic field perpendicular to the container. Figure 1 shows the experimental setup used in the experiments. Previously to the experiments, particles were subjected to the magnetic field for 1 h to assure that during the experiments no further changes in the behavior of the particles in the system were observed. The applied magnetic field is a superposition of a constant component and a sinusoidal component given by

$$B = B_c + B_o \sin(2\pi f t), \tag{1}$$

where B_c is a static magnetic field fixed at 75 G, B_o and f are, respectively, the amplitude and frequency of the unsteady part of the magnetic field. B_o takes values from 0 G to 66 G, and f is kept at 9.25 Hz. The steady component of the magnetic field prevents particles from forming chains and crystals as particles did in Refs. [18,19]. Trajectories of the particles were obtained using ImageJ and its plugin Mosaic [20], and from these, the mean square displacement, W, was determined. We also used ImageJ to obtain the radial distribution function $g(r)$

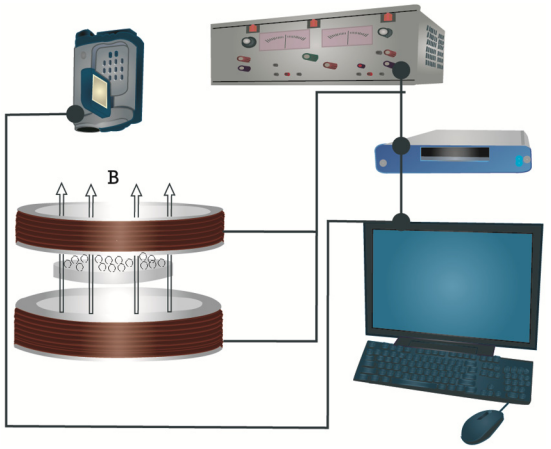

FIG. 1. Scheme of the experimental setup.

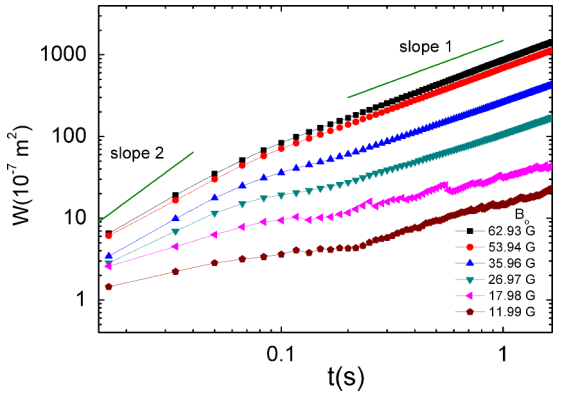

FIG. 2. Mean squared displacement immediately after the system was quenched ($\phi_s = 0.0591$). Each curve corresponds to a different final temperature. Note the linear behavior of the curves corresponding to high temperatures. At low temperatures, the emergence of a plateau indicates an arrested behavior in the system.

and the effective potential $U_E(r)$, we used image stacks to obtain average values.

The mechanism for the energy input and the randomizing of particle motion is described elsewhere [10,21–23] and it differs from the mechanism observed in vibrating systems [7,24]. In brief, when a vertical sinusoidal magnetic field is turned on, a particle tends to align with the magnetic field to reach a minimum potential magnetic energy. When the field decreases, the energy also decreases and eventually, the field points in the opposite direction. In this new condition, the magnetic energy is at a maximum and its absolute values increases, therefore the particle rolls to align again with the magnetic field. Since a sphere has a neutral equilibrium, when it is on a horizontal plane, the rolling direction is random, leading to very complex dynamics. Eventually, the particle meets the initial condition again aligning with the magnetic field, and then it rolls again in a new unpredictable direction. For high frequencies (greater than 30 Hz), there is no motion in most of the particles because of rotational inertia; and for low frequencies, the motion is not continuous. While rolling, magnetic energy is transformed into kinetic energy of the beads, at the same time, part of this energy is lost by friction with the container and through collisions with other particles. Although energy is quickly lost, it is compensated by the energy provided by the unsteady magnetic field, preventing particle motions from stopping. The system is not in thermodynamic equilibrium, however, it does reach a stationary state. In this condition, particle behavior can be described by the Ornstein-Uhlenbeck stochastic model, that is, particles behave as Brownian particles [21]. The effective temperature is controlled by the intensity of the unsteady part of the magnetic field B_o [10,21–23]. Hereafter, B_o is referred to as the effective temperature.

III. FRAGILITY

We carried out quenching experiments from the same initial effective temperature B_o to a final state with lower temperature. Figure 2 shows the behavior of the W obtained for a particle concentration $\phi_s = 0.0591$, in a time window of 1.66 s immediately after the system was quenched. Each curve corresponds to a different final temperature. As expected, as the temperature decreases, W decreases. In each curve it is observed that at the beginning, the particles show a ballistic behavior, i.e., the dependence of W with time is quadratic, then, it becomes linear, showing that particle motion is diffusive. According to the Einstein relation, in the diffusive regime in a two-dimensional (2D) system, $W = 4Dt$, where D is the diffusion coefficient.

Figure 3 shows the diffusion coefficient as a function of the effective temperature for different particle concentrations. It can be observed that as the temperature increases, D remains low until the temperature is higher than a threshold value, then the D values grow quickly as the temperature increases; thus, there are two temperature regimes, low and high. We determine linear fitting curves for the D values in both the high and low temperature regimes for each curve (not shown in the figure), and we identified its intersection as the glass transition temperature B_{og}.

According to the Stokes-Einstein equation, in a fluid, the effective viscosity is proportional to T_E/D. In our granular system T_E is proportional to B_o. In Fig. 4, we plot log (B_o/D) as a function of B_{og}/B_o for several particle concentrations, where B_{og} is the magnetic field when the glass transition

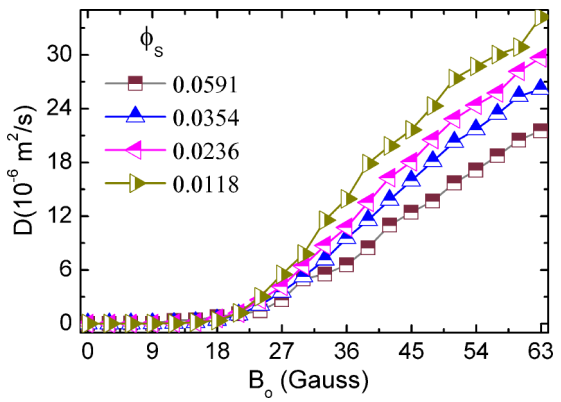

FIG. 3. Diffusion coefficient as a function of the temperature, for some particle concentrations.

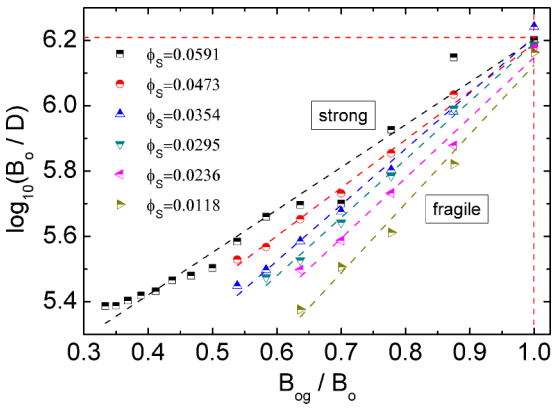

FIG. 4. $\log(B_o/D)$ as a function of B_{og}/B_o exhibits the same behavior to that of classical Angell plots for glass-forming liquids of different fragilities: for high concentrations the system behaves as strong glass-forming liquid, while at low concentrations it behaves like fragile glass-forming liquid.

occurs. We only show the data near the glass transition, the straight lines are linear fittings. These fittings show how fast the slowing down of the dynamics as a function of the effective temperature is when it approaches to B_{og}. We determined the fragility index by using the definition

$$m \equiv \left.\frac{d[\log\,(B_o/D)]}{d(B_{og}/B_o)}\right|_{B_o=B_{og}}. \tag{2}$$

According to Eq. (2), the slope of linear fittings corresponds to the fragility index values. We observed that the fragility of the system depends on particle concentration. Figure 5 depicts the fragility index for different particle concentrations. As it is observed, the fragility index is inversely proportional to particle concentration: the system goes from a fragile to a strong glass-forming liquid behavior with increasing particle concentration. For high particle concentrations, the inverse of the temperature increases at the same rate as $\log(B_o/D)$ far from the glass transition, which is characteristic of strong glass-forming liquids, an Arrhenius behavior. The Arrhenius behavior in this case is due to strong interactions because of the closeness between particles and the repulsive interactions

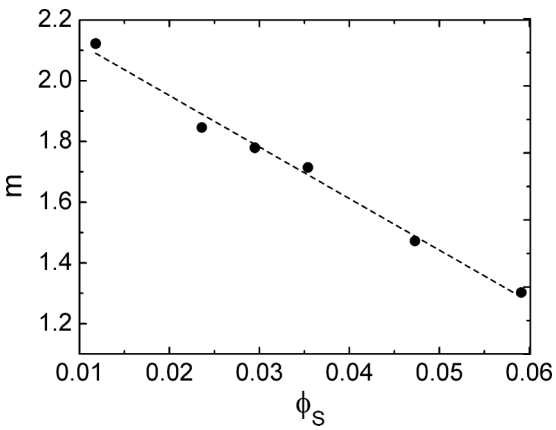

FIG. 5. Fragility index, m, is inversely proportional to particle concentration.

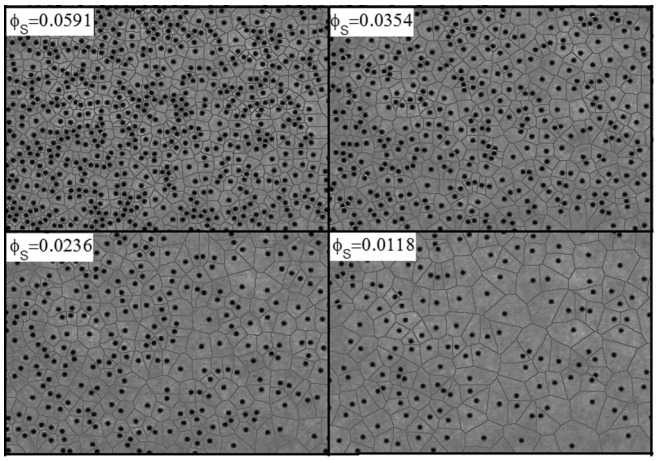

FIG. 6. Snapshots of the system for several particle concentrations and their corresponding Voronoi polygons. The snapshots were taken after the quench.

among them. In samples with low particle concentration, as the inverse of the temperature increases, $\log(B_o/D)$ increases slowly at first, and then, there is a sudden increase as the inverse of the temperature is approaching to the glass transition. This behavior is typical of fragile glass-forming liquids, where particles are less correlated with their neighbors. From this, we conclude that the dynamics of the system is affected by the length of spatial correlations. The structural characteristics must be reflected by the degree of order in the configurations.

IV. REGULARITY FACTOR

We are using Voronoi polygon area distributions to characterize the structural arrangement of particles in our system and its dependence on the effective temperature and particle concentration. Figure 6 shows snapshots of samples with different particle concentration and their corresponding Voronoi polygons. For low particle concentrations, there are few polygons and the area distribution is wide. For samples with high particle concentration, the distribution is narrow because large polygons are restricted due to the closeness of the particles. Voronoi polygon areas Λ were measured in a sequence of 1000 frames for each particle concentration. We obtain the Voronoi free area distributions normalized with the area of the Voronoi polygon corresponding to the close packing hexagonal lattice $\Lambda_{\rm hex}$. The Voronoi free area is defined as $\Lambda - \Lambda_{\rm hex}$. We defined the normalized free area as X. Figure 7 shows a comparison between the normalized Voronoi polygon area distributions for two particle concentration, $\phi_s = 0.0591$ and $\phi_s = 0.0118$. We have excluded Voronoi polygons on the edge of the observation area to avoid edge effects. As one can see here, for low particle concentration, the Voronoi free area distribution spans over a wider range of values. On the other hand, for the higher particle concentration, the polygons are smaller and the distribution becomes narrower, exhibiting a well-defined main peak. The position of the main peak shifts toward lower values as particle concentration increases, approaching the position of zero (the hexagonal lattice) but still having a non-vanishing width, i.e., the system approaches to more ordered structure as particle concentration increases.

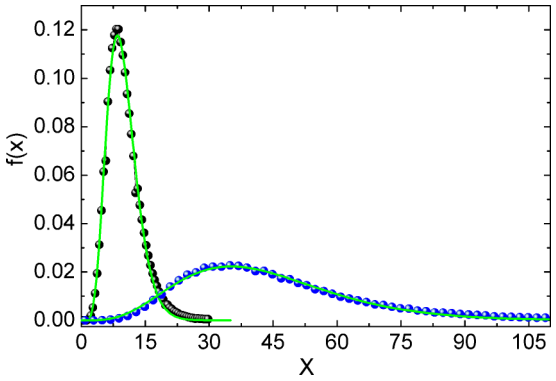

FIG. 7. Voronoi area distributions for the highest $\phi_s = 0.0591$ (black spheres), and the lowest particle concentration $\phi_s = 0.0118$ (blue spheres), both at high temperature. Solid lines are fits to two-parameter γ distributions.

In Refs. [25–28] have been shown that the distribution of the individual Voronoi free area in related systems can be well fitted by two and three-parameter γ distributions. A two-parameter γ distribution is given by

$$f(X) = (\beta^{-\alpha}/\Gamma(\alpha))X^{\alpha-1}\exp(-X/\beta), \tag{3}$$

where α and β are constants, α is called the regularity factor. The regularity factor has been used as a measure of the structural order. It is a measure of how the distributions spread, where a sharper distribution indicates a more regular structure. This parameter, as a function of the effective temperature shows significant changes when the system freezes. Figure 8 shows the regularity factor as a function of the inverse of the effective temperature for different particle concentration. It can be observed that as the effective temperature decreases, the regularity factor increases. Around a threshold value, the curve stops increasing and the values start decreasing. Thus, this threshold can be used to determine the temperature where important structural changes appear. For higher particle concentrations, the transition is very clear and sharp. As particle concentration decreases, the transition becomes diffuse, but it is clear that a change occurs. Figure 9 shows

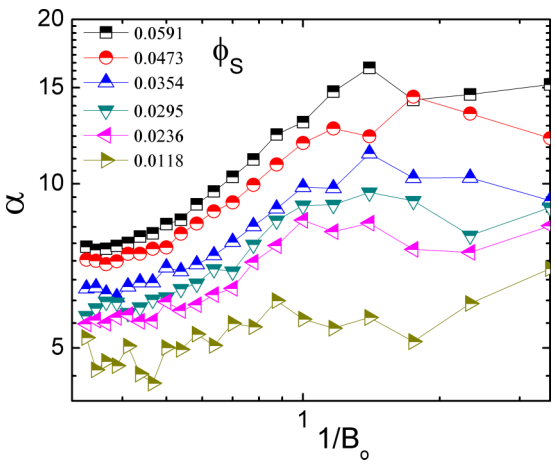

FIG. 8. Regularity factor as a function of the inverse of the temperature.

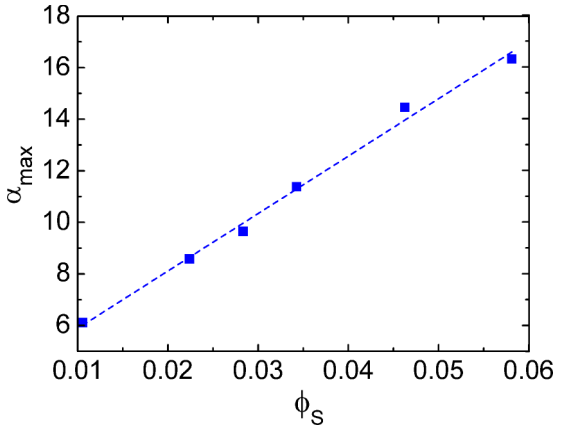

FIG. 9. The maximum of the regularity factor, α_{max}, as a function particle concentration.

the maximum peak α_{max} of each curve of the regularity factor for the different particle concentrations.

V. ANALYSIS

From Figs. 5 and 9 which show the behavior of fragility index and the maximum of the regularity factor as functions of the particle concentration, we obtained Fig. 10. This figure shows an important relation between fragility index and the regularity factor and it constitutes the main result of this work. A strong glass forming system is more ordered than a fragile glass forming system.

Now we proceed to calculate the effective potential to discuss our result in terms of spatial correlations. First, we determined the radial distribution function for several temperatures at each particle concentration. Then, from these curves we obtain the effective potential. The procedure to obtain the effective potential is described elsewhere [10,23]. In brief, the procedure is as follows. It starts with the use of the two dimensional version of the Ornstein-Zernike equation [29]

$$h(r_{12}) = c(r_{12}) + \rho \int d^2\mathbf{r}_2\, c(r_{13})h(r_{32}), \tag{4}$$

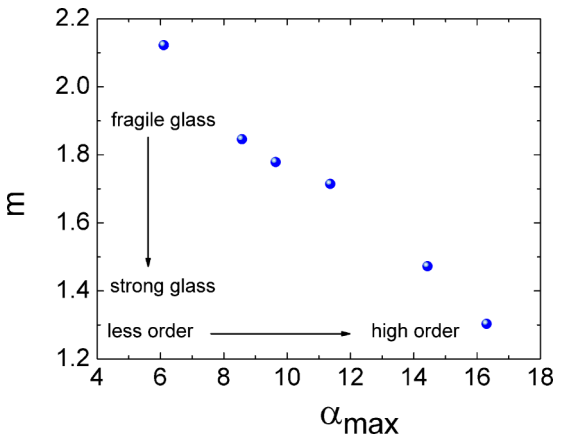

FIG. 10. Fragility index as a function of the maximum of the regularity factor for the cases we analyzed.

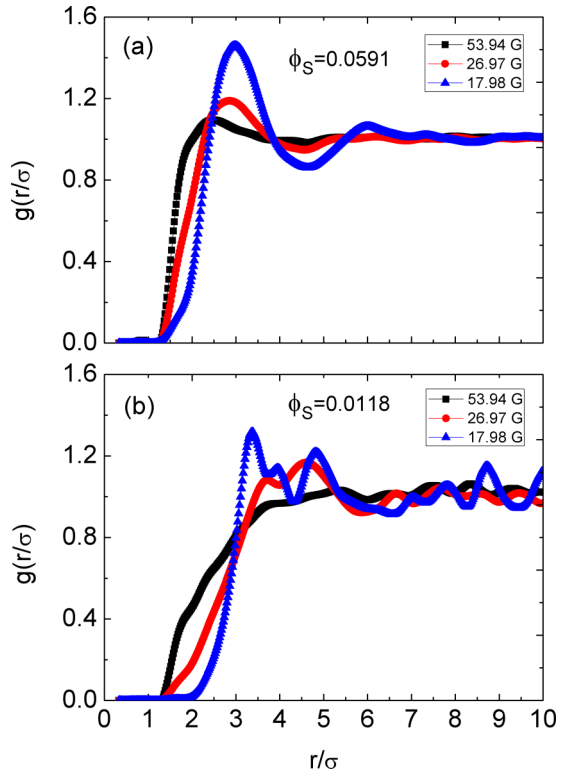

FIG. 11. (a) Radial distribution function for the highest $\phi_s = 0.0591$ and (b) the lowest particle concentration $\phi_s = 0.0118$, for different temperatures.

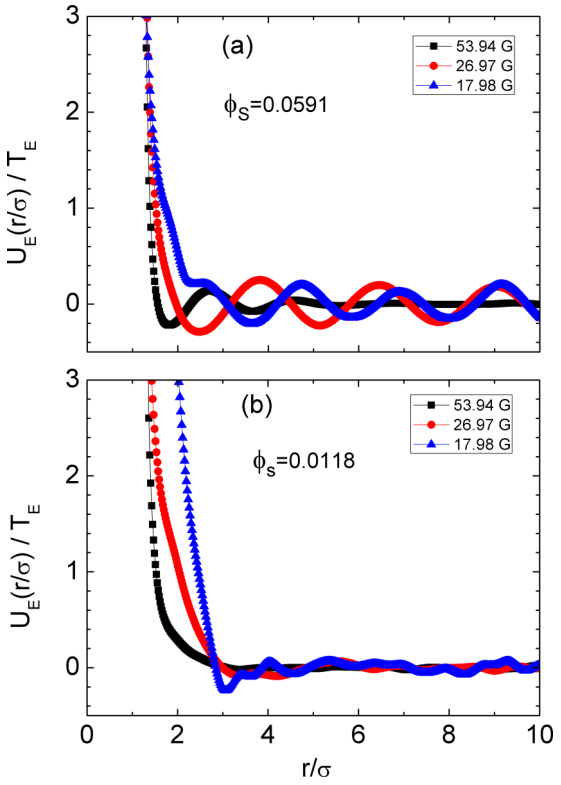

FIG. 12. Effective potential for the highest (a) and the lowest concentration (b).

where $\rho = N/A$ is the average number of particles in the field of view. In Eq. (4), $h(r) = g(r) - 1$ is the correlation function and $c(r)$ is the direct correlation function. By taking the Fourier transform of Eq. (4), we obtain an algebraic expression for $\hat{c}(k)$ in terms of $\hat{h}(k)$,

$$\hat{c}(k) = \frac{\hat{h}(k)}{1 - \rho\hat{h}(k)}. \tag{5}$$

Using the experimental values of $h(r)$, we can obtain $\hat{h}(k)$ and then by using Eq. (5) we can obtain $\hat{c}(k)$. Now, $\hat{c}(k)$ is transformed back to the real space to get the direct correlation function $c(r)$. The hypernetted chain, among other closure relations, establishes an approximate relationship between $c(r)$ and the effective potential $U_E(r)$, that is [30],

$$h(r) - c(r) = \ln g(r) + U_E(r)/T_E. \tag{6}$$

This can be solved for $U_E(r)/T_E$. T_E is the effective temperature expressed in energy units, as we stated previously, this is proportional to B_o. For the purpose of the qualitative discussion of our result in terms of the effective potential, it is enough to plot $U_E(r)/T_E$.

Figure 11 shows $g(r/\sigma)$ curves at different temperatures for a high particle concentration, $\phi_s = 0.0591$ [Fig. 11(a)], and a low particle concentration, $\phi_s = 0.0118$ [Fig. 11(b)]. In the high particle concentration, as the temperature decreases, the $g(r)$ curves evolves from a gas state where a depletion zone is observed because of particle repulsive interactions, to a liquid state due to local tendency toward ordered particle configurations. In the case of low particle concentration, the radial distribution shows a diffuse local order that almost does not change as temperature goes down. Figure 12(a) shows the respective effective potential curves for the larger particle concentration case. The appearance and evolution of a well that is responsible of the local order as temperature goes down can be observed. This well becomes deeper and sharper as the temperature goes down and at the same time others wells appear and evolve in a similar way. This means that the range of interaction is larger as the temperature goes down. By contrast, in Fig. 12(b), for the low particle concentration case, it can be observed that the effective potential also shows a short distance of interaction and that the wells are diffuse. In this case, the range of interaction remains relatively short and cannot drive the system to more ordered configurations.

VI. COMMENTS AND REMARKS

In this work, we found that our magnetically agitated 2D particle system goes from a fragile to a strong glass-forming liquid behavior as particle concentration increases. We observe that fragile glass-forming behavior is associated with lower local order compared with a strong glass-forming behavior where the local order is more notable. Thus, fragility and local order depends upon particle concentration and in turn this controls the length and intensity of the effective interaction. As the length of interaction lengthens and strengthens, the fragility decreases leading the system to a strong glass-forming liquid behavior and to a more ordered configuration. This result is accord with recent results based on the study of hyperuniformity which claims that strong

glass-forming liquid presents a more hyperuniformity than a fragile glass-forming liquid [31], if we consider the uniformity represents more order in the system. In Ref. [9] is studied a system based on a soft colloidal system, the main results basically are that soft colloids make strong glass-forming systems and hard spheres make fragile glass-forming systems, and that the elasticity of the system is directly related with the fragility. When using soft colloids, because the particles are deformable to reach a glass transition it is needed a higher particle concentration than using hard particles. That is, higher particle concentrations make strong glass-forming systems according to our results. Finally, this system could also be used to carry out experiments modifying the intensity of the interaction through the magnetic interaction intensity.

ACKNOWLEDGMENTS

Partial financial support by Soft Condensed Matter RED TEMATICA and by CONACyT, México, through Grants No. 256176 (SEP-Ciencia Básica) and No. 440 (Fronteras de la Ciencia) is acknowledged.

[1] E. R. Weeks, J. C. Crocker, A. C. Levitt, A. Schofield, and D. A. Weitz, Science **287**, 627 (2000).
[2] E. R. Weeks, J. C. Crocker, and D. A. Weitz, J. Phys.: Condens. Matter **19**, 205131 (2007).
[3] G. L. Hunter and E. R. Weeks, Rep. Prog. Phys. **75**, 066501 (2012).
[4] H. König, R. Hund, K. Zahn, and G. Maret, Eur. Phys. J. E **18**, 287 (2005).
[5] A. R. Abate and D. J. Durian, Phys. Rev. Lett. **101**, 245701 (2008).
[6] L. J. Daniels, T. K. Haxton, N. Xu, A. J. Liu, and D. J. Durian, Phys. Rev. Lett. **108**, 138001 (2012).
[7] P. M. Reis, R. A. Ingale, and M. D. Shattuck, Phys. Rev. Lett. **98**, 188301 (2007).
[8] P. M. Reis, R. A. Ingale, and M. D. Shattuck, Phys. Rev. E **75**, 051311 (2007).
[9] J. Mattsson, H. M. Wyss, A. Fernandez-Nieves, K. Miyazaki, Z. Hu, D. R. Reichman, and D. A. Weitz, Nature **462**, 83 (2009).
[10] C. Tapia-Ignacio, J. Garcia-Serrano, and F. Donado, Phys. Rev. E **94**, 062902 (2016).
[11] H. W. Sheng, W. K. Luo, F. M. Alamgir, J. M. Bai, and E. Ma, Nature **439**, 419 (2006).
[12] H. G. E. Hentschel, V. Ilyin, N. Makedonska, I. Procaccia, and N. Schupper, Phys. Rev. E **75**, 050404(R) (2007).
[13] Y. Song, Z. Wang, L. Zhao, and J. Luo, Mater. Des. **31**, 4281 (2010).
[14] T. Aste, K. Y. Szeto, and W. Y. Tam, Phys. Rev. E **54**, 5482 (1996).
[15] A. Soyer, J. Chomilier, J. P. Mornon, R. Jullien, and J. F. Sadoc, Phys. Rev. Lett. **85**, 3532 (2000).
[16] A. Poupon, Curr. Opin. Struct. Biol. **14**, 233 (2004).
[17] M. Wu, F. Xiao, R. M. Johnson-Paben, S. T. Retterer, X. Yin, and K. B. Neeves, Lab Chip **12**, 253 (2012).
[18] D. L. Blair and A. Kudrolli, Phys. Rev. E **67**, 021302 (2003).
[19] L. Oyarte, P. Gutiérrez, S. Aumaitre, and N. Mujica, Phys. Rev. E **87**, 022204 (2013).
[20] I. F. Sbalzarini and P. Koumoutsakos, J. Struct. Biol. **151**, 182 (2005).
[21] F. Donado, R. E. Moctezuma, L. López-Flores, M. Medina-Noyola, and J. L. Arauz-Lara, Sci. Rep. **7**, 12614 (2017).
[22] R. E. Moctezuma, J. L. Arauz-Lara, and F. Donado, Physica A (Amsterdam) **496**, 27 (2018).
[23] F. Donado, J. M. Sausedo-Solorio, and R. E. Moctezuma, Phys. Rev. E **95**, 022601 (2017).
[24] S. Merminod, M. Berhanu, and E. Falcon, Europhys. Lett. **106**, 44005 (2014).
[25] V. S. Kumar and V. Kumaran, J. Chem. Phys. **123**, 114501 (2005).
[26] T. Aste and T. Di Matteo, Phys. Rev. E **77**, 021309 (2008).
[27] I. Schenker, F. T. Filser, L. J. Gauckler, T. Aste, and H. J. Herrmann, Phys. Rev. E **80**, 021302 (2009).
[28] T. Aste, G. W. Delaney, and T. Di Matteo, in *IUTAM-ISIMM Symposium on Mathematical Modeling and Physical Instances of Granular Flows*, edited by J. Goddard, J. T. Jenkins, and P. Giovine, AIP Conf. Proc. No. 1227 (AIP, Melville, NY, 2010), p. 157.
[29] J. P. Hansen and I. R. McDonald, *Theory of Simple Liquids*, 2nd ed. (Academic, New York, 1986).
[30] D. A. McQuarrie, *Statistical Mechanics* (University Science Books, Sausalito, CA, 2000).
[31] G. Zhang, F. H. Stillinger, and S. Torquato, Sci. Rep. **6**, 36963 (2016).